

NONLINEAR FINITE ELEMENT 2D ANALYSIS FOR RC BEAMS STRENGTHENED BY EPOXY BONDED STEEL PLATES

Wen-Shan Lin *

Architecture & Building Research Institute
Ministry of Interior
Taipei, Taiwan 106, R.O.C.

Chen-Chang Kao **

Department of Civil Engineering
National Taiwan University
Taipei, Taiwan 10617, R.O.C.

ABSTRACT

This paper presents the nonlinear finite element modeling of the global behavior for RC beam strengthened by externally epoxy bonded steel plates up to failure. In addition to the consideration of nonlinear behavior and cracking of concrete, the model involves interface element to capture not only the shear and normal stress concentration at the plate curtailment, but also the separation due to the exceeded peak shear and normal stress. The internal steel bar using truss element and the external steel plate using deformation theory of plastic have been confirmed by compare finite element solution with plastic theory. The proposed finite element solutions result in close correlation with experimental data available for RC beams strengthened by epoxy bonded steel plates with different thickness.

Keywords : Nonlinear finite element, Interface element, Strengthened RC beam.

1. INTRODUCTION

RC structure must be repaired or strengthened when the behavior of RC structures is found to be inadequate. The inadequacy may be due to inferior materials, design, or constructional fault. Deteriorated RC structures need to be repaired to extend their useful service life. Strengthening and repair of RC members by steel plates externally bonded to the tension face of the members is a common technique that has been studied by many investigators [1,2], and many structures have been successfully strengthened in flexure using this technique [3,4]. The successful strengthened structure must remain full composite action until failure in ductile manner. The peak shear and normal stress will be developed at plate curtailment under loading, the plate separation occurs immediately if the peak shear and normal stress exceeds the strength of interface. Many researches [5,6] have analyzed the plated RC beam using strength of material approach. However, the linear behavior of all component materials is assumed in above approach.

In this present study, the nonlinear finite element modeling of the global behavior of the externally reinforced RC beam up to failure is developed. The model involves interface element to capture the characteristics of the interface between the concrete and external plates.

2. MATERIAL MODEL AND CONSTITUTIVE RELATIONSHIP

2.1 Concrete

Tension

In the present study, the stress-strain relationship under tension is assumed linear with initial elastic modulus of concrete up to the maximum tensile stress f'_t . After crack occurs, the stress is reduced to a value determined by the tension stiffening parameter. The value of f'_t in this study is taken from the equation proposed by Raphael [7] as

$$f'_t = 0.7(f'_c)^{2/3} \quad (1)$$

Equation (1) is in unit of kg/cm^2 .

Tension Stiffening

The "tension stiffening" has to be incorporated into a cracking model to correctly simulate the load carrying capacity of a reinforced member in tension. Many investigators [8,9] have proposed various stress-strain curves of concrete after cracked. The stress-strain relation used is shown in Fig. 1 [10]. When a crack occurs, the stress normal to the crack can be obtained as follows:

$$\sigma_i = \alpha f'_t \left(1 - \frac{\varepsilon_i}{\varepsilon_m} \right) \quad (2)$$

and the secant modulus E_i is

* Postdoctoral Researcher

** Professor Emeritus

$$E_i = \alpha f'_t \left(1 - \frac{\varepsilon_i}{\varepsilon_m} \right) \frac{1}{\varepsilon_i} \quad (3)$$

where α and ε_m are tension stiffening parameters, and ε_i is current strain in i direction.

The tension stiffening parameter α was calibrated against compressive strength f'_c . In the present study, the value of α was determined according to Mphonde's experimental studies of beams without stirrups [11]. Cracking strain beyond the one represented by parameter ε_m , which stress can not be carried across the cracks. The value of ε_m was assumed constant at 0.002 in this study.

Shear Degradation

After crack occurs, the dowel effect and aggregate interlocking can be incorporated into a continuum model by using equivalent shear stiffness. Test [12] has shown that the primary variable in the shear transfer mechanisms is the crack width. Many investigators reduce a shear modulus of uncracked concrete to simulate dowel action and aggregate interlocking. In the present study, the shear modulus of cracked concrete is assumed to be function of the current principal tensile strain [13]. The shear degradation of cracked concrete can be described as follow

$$G^c = \begin{cases} 0.25G (1 - \varepsilon_1/0.005) & \varepsilon_1 \leq 0.005 \\ 0 & \varepsilon_1 \geq 0.005 \end{cases} \quad (4)$$

where G is the shear modulus of uncracked concrete, and ε_1 is the tensile strain in the normal to cracked direction. In numerical, G^c set to $0.001G$ when ε_1 is higher than 0.005. For concrete cracking in both directions, the shear modulus calculated by using Eq. (4) with reduced 50 percent.

Biaxial Concrete Strength

Under combination of biaxial loading, concrete strength and stress-strain behavior is different from that under uniaxial loading conditions. Many investigators have proposed the mechanical properties of concrete under biaxial loading. In this study, the concrete strength is determined using the failure envelope proposed by Kupfer and Gerstle [14].

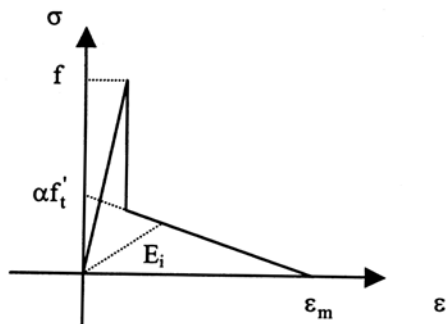


Fig. 1 Tension stiffening behavior of cracked concrete

An Equivalent Uniaxial Stress-Strain Relationship

The secant modulus with different stress levels will be used to describe the stress-strain relationship under multi-direction stresses. The stress-strain curve (Fig. 2) in compressive is approximated by the following expression proposed by Guo *et al.* [15]:

$$\beta_i = 2.2 x_i - 1.4 x_i^2 + 0.2 x_i^3 \quad (5)$$

where $\beta_i = \frac{\sigma_i}{\sigma_{if}}$ denotes the nonlinearity index for current stress state for i principal direction, and x_i is the ratio of current strain to corresponding strain at failure stress for i principal direction, which can be described as follows,

$$x_i = \frac{\varepsilon_i}{\varepsilon_{ip}} = \frac{\sigma_i / E_{is}}{\sigma_{if} / E_{if}} = \beta_i \frac{E_{if}}{E_{is}} \quad (6)$$

where $E_{is} = \sigma_i / \varepsilon_i$ is the secant modulus of current stress level; $E_{if} = \sigma_{if} / \varepsilon_{ip}$ is the secant modulus for strength level; and σ_{if} is concrete strength in i direction under multi-direction stresses.

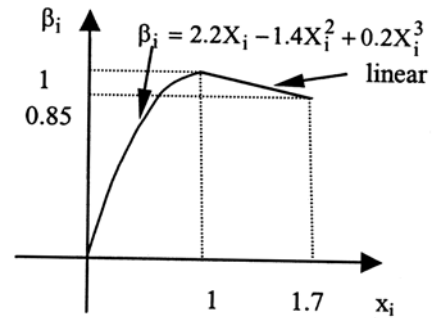


Fig. 2 Compression behavior of concrete

Using simple algebra, Eq. (5) can be solved to obtain the actual secant modulus E_{is} for i principal direction. The expression for E_{is} contains the actual stress in terms of the nonlinearity index β_i . Substituting Eq. (6) into Eq. (5), we obtain

$$2.2 \frac{E_{if}}{E_{is}} - 1.4 \beta_i \left(\frac{E_{if}}{E_{is}} \right)^2 + 0.2 \beta_i^2 \left(\frac{E_{if}}{E_{is}} \right)^3 - 1 = 0 \quad (7)$$

Set

$$r = E_{if} / E_{is} \quad (8)$$

$$f(r) = 2.2 r - 1.4 \beta r^2 + 0.2 \beta^2 r^3 - 1 \quad (9)$$

and its derivative

$$f'(r) = \frac{df}{dr} = 2.2 - 2.8 \beta_i r + 0.6 \beta_i^2 r^2 \quad (10)$$

Solve Eq. (7) using Newton-Raphson method. Let the initial value r_1 equal to 1 at first iteration step. After the $k+1$ th iteration, the value of r_{k+1} can be determined as follows,

$$r_{k+1} = r_k - \frac{f(r_k)}{f'(r_k)} = r_k - \frac{2.2r_k - 1.4\beta_i r_k^2 + 0.2\beta_i^2 r_k^3 - 1}{2.2 - 2.8\beta_i r_k + 0.6\beta_i^2 r_k^2} \quad (11)$$

Iteration will be terminated when $|r_{k+1} - r_k|$ is smaller than a prescribed tolerance. The secant modulus with different stress levels has been found as follows;

$$E_{is} = \frac{E_{if}}{r_{k+1}} = \frac{E_{i0}}{2.2r_{k+1}} \quad (12)$$

where E_{i0} = initial modulus. The value of E_{i0} in this study is taken from the equation proposed by ACI committee 363 [16] and Massicottee *et al.*, [17] as

$$E_0 = 10600 \sqrt{f'_c} + 70336 \quad (13)$$

where concrete strength f'_c ranging from 214kg/cm² to 846kg/cm².

After finding the secant modulus, the orthotropic constitutive law can be established by using total stress-strain relationship. This method describes the restrictions on the ascending portion of the stress-strain curve under proportional loading. For descending portion of stress-strain curve, we assume linear relation until failure, which defined stress reducing 0.85 times strength and strain increasing 1.75 times strain corresponding with strength. After crack occurs, the secant modulus was determined according to tension stiffening effect in the direction perpendicular to the crack. For direction parallel to the crack as subjected to tension, it hardly has influence on the secant modulus with assuming linearity. Beside, for direction parallel to the crack as subjected to compression, the softened concrete phenomenon would happen.

The Softened Concrete in Biaxial Tension-Compression

After cracking, the stress-strain relationship for biaxial tension-compression will be considered. For tension along perpendicular cracking direction, the "tension stiffening" effect may occur which has been explained previously. For compression along parallel cracking direction, the stress-strain relationship is the softening of peak stress in comparison to the standard cylinder. Many investigators [18~20] tested panels subjected to biaxial stresses, and confirmed that the compressive strength of reinforced concrete can be softened by the tensile strain in the perpendicular direction. In the present study, the softening coefficient is approximated by the following expression proposed by Belarbi and Hsu [20].

$$\xi = \frac{0.9}{\sqrt{1 + 400 \varepsilon_r}} \quad (14)$$

where ε_r is the tensile strain perpendicular to the cracking direction.

The stress-strain relation for compression along the direction parallel to cracking can be modified by replacing f'_c with $\xi f'_c$ and ε_0 with $\xi \varepsilon_0$ in Eq. (5).

Constitutive Relationship of Concrete

To simulate the stress state of concrete under biaxial loading, the orthotropic model [21] is adopted in this study. The orthotropic direction coincides with principal stress direction for uncracked concrete and these conditions are parallel and normal to the cracks for the cracked concrete. The stress-strain relations are first defined in the axes of orthotropic direction and are then transformed to the global coordinate system by a rotation transformation. The local material stiffness with the form as

$$[D]_{Lo} = \frac{1}{1-\nu^2} \begin{bmatrix} E_1 & \nu\sqrt{E_1 E_2} & 0 \\ \nu\sqrt{E_1 E_2} & E_2 & 0 \\ 0 & 0 & \frac{1}{4}(E_1 + E_2 - 2\nu\sqrt{E_1 E_2}) \end{bmatrix} \quad (15)$$

where E_1 and E_2 = secant modulus in principal direction 1 and 2, respectively; and ν = Poisson's ratio. When the biaxial compressive stress exceeds Kupfer's failure envelope, concrete enter the region of strain softening. In this region, failure occurs by crushing of concrete when the principal compressive strain exceeds a limit value ε_{iu} .

In this study, a smeared cracked model was adopted for describing the behavior of cracked concrete. The material axes are fixed after formation of the initial crack. It is called the "fixed cracked model". In this model the initiation of a cracking process at any Gauss point happens when the concrete stress reaches the equivalent tensile strength. In the modeling of cracking of concrete, the following are considered: (1) tension stiffening effect, (2) shear degradation, and (3) concrete softening effect. After single crack take place, the concrete is treated as an orthotropic material with principal axes normal and parallel to the cracking direction. The Poisson's ratio was neglected. Thus, the concrete material stiffness matrix with respect to the cracking direction can be given by

$$\begin{Bmatrix} \sigma_1 \\ \sigma_2 \\ \tau_{12} \end{Bmatrix} = \begin{bmatrix} E_1 & 0 & 0 \\ 0 & E_2 & 0 \\ 0 & 0 & G_{12}^c \end{bmatrix} \begin{Bmatrix} \varepsilon_1 \\ \varepsilon_2 \\ \gamma_{12} \end{Bmatrix} \quad (16)$$

where E_1 is the secant modulus for crack direction, E_2 is the secant modulus for uncracked, and G_{12}^c is shear degradation modulus.

When the second crack develops in the orthogonal direction for σ_2 reaching equivalent tensile strength, the material matrix should be modified as

$$\begin{Bmatrix} \sigma_1 \\ \sigma_2 \\ \tau_{12} \end{Bmatrix} = \begin{bmatrix} E_1 & 0 & 0 \\ 0 & E_2 & 0 \\ 0 & 0 & \frac{1}{2}G_{12}^c \end{bmatrix} \begin{Bmatrix} \varepsilon_1 \\ \varepsilon_2 \\ \gamma_{12} \end{Bmatrix} \quad (17)$$

where E_1 and E_2 are the secant modulus for cracked direction.

Similarly, the material matrix for cracked concrete in the coordinate system of crack must also be transformed into to the form in the global coordinate system.

2.2 Reinforcing Steel Bar

A one-dimensional elastic-plastic material model in both compression and tension is adopted for describing the behavior of the internal flexural and shear steel reinforcements. The yielding is determined by the uniaxial yield stress σ_y and further loading results in the elastic-plastic behavior with linear strain hardening. The secant modulus \bar{E}_s before yielding is

$$\bar{E}_s = E_s \quad (18)$$

and after yielding is

$$\bar{E}_s = \frac{f_s}{\varepsilon_s} \quad (19)$$

where

$$f_s = \sigma_y + E_{sp}(\varepsilon_s - \varepsilon_y) \quad (20)$$

for tensile, and

$$f_s = -\sigma_y + E_{sp}(\varepsilon_s + \varepsilon_y) \quad (21)$$

for compression, where E_{sp} denote the strain hardening modulus.

2.3 External Steel Plate

A two-dimensional elastic-perfectly-plastic material model in both compression and tension is adopted in this study to simulate the behavior of the external bonded plate. There are two types of theory dealing with plastic material, namely, the deformation theory of plasticity and incremental theory of plasticity. The deformation and incremental theories of plasticity use the secant and tangent modulus, respectively. In the present study, the deformation theory is adopted because it is consistent with other material models that use secant modulus. The procedure of the constitutive law of deformation theory can be found in Ref. [22].

2.4 Concrete/Glue/Plate Interface

The interface material is modeled by a linear-elastic-fracture relationship (Fig. 3). Prior to the cracking of the interface, the material is assumed to be isotropic. Due to its special thin geometry, the interface element can crack only along the glue line or perpendicular to it [10]. Cracks perpendicular or along the glue line will occur as soon as the corresponding

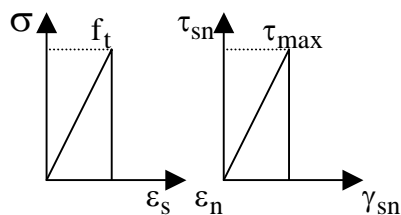


Fig. 3 Material behavior of the interface element in tension and shear

normal stress reaches the tensile strength of the interface. After cracking, the elasticity modulus in the corresponding direction is set to zero. The Poisson's ratio was neglected. The shear modulus reduces to 0.25 times of uncracked value [10]. If the crack is perpendicular to the glue line, the updated material matrix for the interface becomes

$$[D]_{s-n} = \begin{bmatrix} 0 & 0 & 0 \\ 0 & E_g & 0 \\ 0 & 0 & 0.25G_g \end{bmatrix} \quad (22)$$

The interface could also crack parallel the glue line under combined shear and normal stresses, which has been shown in study [23] to follow a Mohr-Coulomb type fracture criterion given by

$$\tau = c - \sigma \tan \phi \quad (23)$$

where cohesion for a concrete / glue / plate interface ranges from 49kg/cm² to 97kg/cm² with $\phi = 28^\circ$ for room temperature. The wide range of cohesion c can be attributed to the variation in surface preparation and properties of the adhesive and concrete. If the normal stress perpendicular to the glue line is tensile at the instant of failure as predicted by Mohr-Coulomb law, which is referred to as the peeling stress, all stress components and elements of the material matrix are reduced to zero. However, if the normal stress perpendicular to the glue line is compressive at the instant of failure as predicted by Mohr-Coulomb law, then only the shear stress and the corresponding the shear modulus are set to zero. In this case, the material matrix is updated to

$$[D]_{s-n} = \frac{E_g}{1 - \nu_g^2} \begin{bmatrix} 1 & \nu_g & 0 \\ \nu_g & 1 & 0 \\ 0 & 0 & 0 \end{bmatrix} \quad (24)$$

3. FINITE ELEMENT MODEL AND SOLUTION CONVERGENCE CRITERIA

3.1 Finite Element Model

Concrete and external plates are presented by eight nodes isoparameter finite element as shown in Fig. 4. Numerical integration for any element was carried out using Gauss-integration technique over nine sampling points. At each iteration of any load, the material

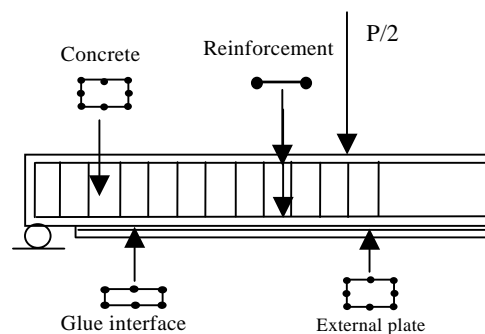


Fig. 4 Finite element model

matrix at every sampling point of the concrete and external are updated and modified to take into account the material nonlinearities as described previously. The internal steel including the main tensile and compressive steel as well as stirrups are modeled using two-node truss element (Fig. 4). Concrete/glue/plate interface element model is using six-node thin interface element (Fig. 4). The six-node thin interface element proposed by Ziraba and Baluch [10].

3.2 Solution Convergence Criteria

A convergence criterion based on the norm of the nodal displacement is selected in this study. The norm of the nodal displacement convergence criterion is selected as follow

$$\lambda = \frac{\max |v_{i+1}| - \max |v_i|}{\max |v_i|} \quad (25)$$

where v_i is the nodal displacement. Iteration will be terminated when λ is smaller than 0.5%.

4. NUMERICAL EXAMPLE AND VERIFICATION

The ability of the numerical model developed in this study to predict the structural response of a reinforced concrete beam externally strengthened by plates with sufficient strength and rigidity is verified. First, the verification of the constitutive model for plane concrete is presented. Second, we plan to verify that the results of two nodes truss element are comparable with the theory of plastic. Third, we will check the deformation theory of plasticity for external plates. Finally, the numerical results of a reinforced concrete beam externally strengthened with plates are compared with experimental data available from Ref. [24].

4.1 Verification of Constitutive Model for Plane Concrete

The comparison results of stress-strain relationship between the analysis predicted and the test results provided by Kupfer [25] and Tasuji [26] are shown in Figs. 5 to 7. Figures 5 shows the uniaxial compression, Fig. 6 and 7 show the biaxial compression under stress ratio of $\sigma_2 / \sigma_3 = 0.5$ and $\sigma_2 / \sigma_3 = 1$, respectively. In all case, the prediction of the stress-strain relationships of concrete was compared well with experimental average data provided by Kupfer and Tasuji.

4.2 Verification of Two Nodes Truss Element

This section intends to compare the results of two nodes truss element with the theory of plastic. The bilinear stress-strain relation of truss element is adopted. The same material properties of all elements are assumed as follow: initial elasticity modulus, $E_s = 2.04 \times 10^6 \text{kg/cm}^2$; tangential modulus after yielding, $E_{sp} = E_s / 20 = 102000 \text{kg/cm}^2$; yielding stress, $\sigma_y = 2800 \text{kg/cm}^2$; and cross section area, $A = 10 \text{cm}^2$. The load-deflection curve

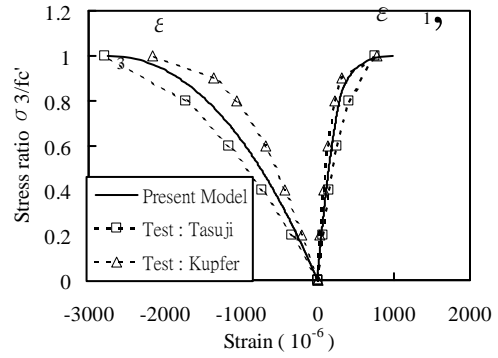


Fig. 5 Stress-strain characteristics under uniaxial compression

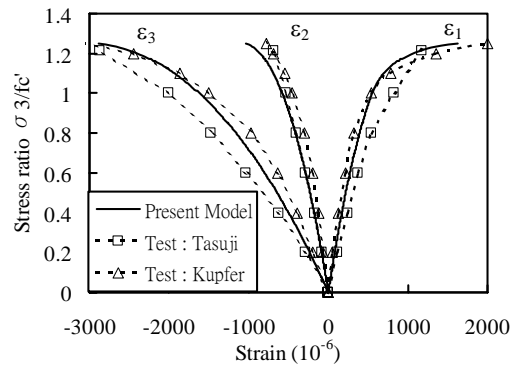


Fig. 6 Stress-strain characteristics under biaxial compression when $\sigma_2 / \sigma_3 = 0.5$

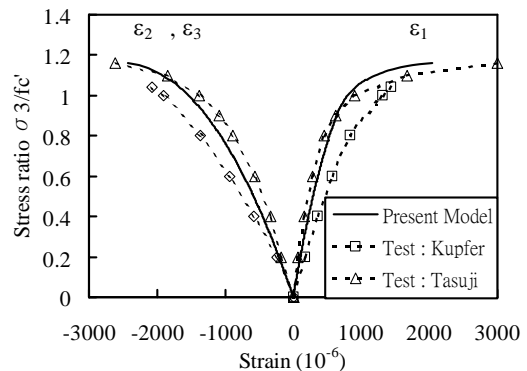


Fig. 7 Stress-strain characteristics under biaxial compression when $\sigma_2 / \sigma_3 = 1$

of this problem is shown in Fig 8. Figure 8 shows the comparison between the numerical and the plasticity theory, and close agreement is indicated. It confirms that the program is correctness for truss element.

4.3 Verification of the Deformation Theory of Plasticity

This section tends to verify the deformation theory of plasticity for external plates. An elastic-perfectly-plastic material model in both compression and tension is assumed. The simple support beam is considered in this verification as shown in Fig 9. Eight nodes element is used to analyze this simple beam. The material

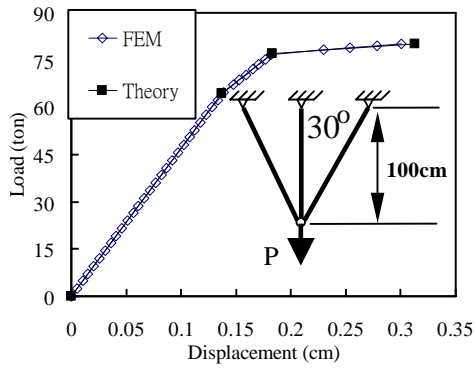


Fig. 8 Load-deflection curve to verify truss element

properties of this beam are assumed as follow: elasticity modulus, $E_s = 2.04 \times 10^6 \text{kg/cm}^2$; yielding stress, $\sigma_y = 2800 \text{kg/cm}^2$; and Poisson's ratio, $\nu = 0.3$.

Figure 9 shows the middle deflection of simple beams under four points loading. As shown in Fig. 9, the elastic stiffness agreed well with that from linear elastic beam theory. The loads of first yield and ultimate were nearly the same as the results by plastic theory. Figure 10 shows the distribution of strain and stress along the height from bottom at a load of 17.5 ton. As shown in Fig. 10, the distribution of strain and stress agreed well with results by plastic theory. It confirms that the program is correct for the deformation theory of plasticity for external plate.

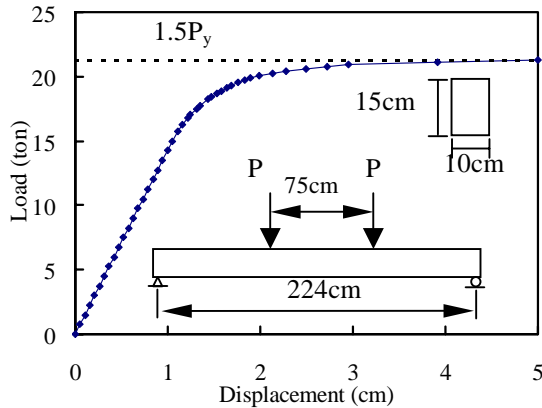


Fig. 9 Load-deflection curve to verify deformation theory

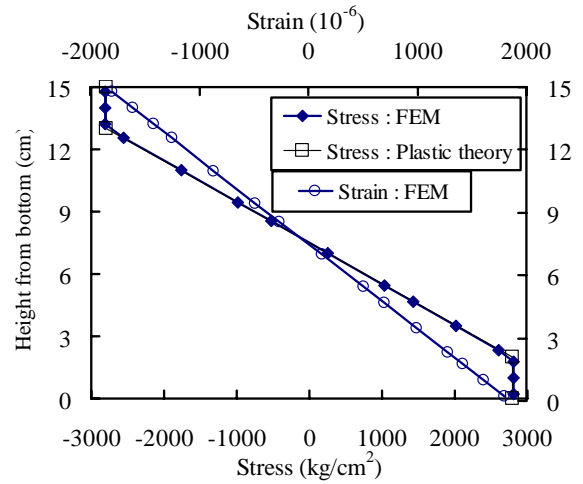


Fig. 10 Stress and strain distribution

4.4 Verification of Beams Strengthened with Steel Plates

To verify the present numerical model with regard to beams strengthened with external steel plate, beams tested in Ref. [24] have been selected. In the following section, the beams details and material characteristics used in the numerical computations are outlined. Comparisons between the numerical and the experimental results are made.

Beam Detail and Material Parameter

Four of the beams have been selected to examine the present numerical model. The beams are URB1, URB2, URB3 and URB4, and the experimental program with detail description and material properties can be found in Ref. [24]. Figure 11 presents an overall summary of the geometry of the beams studies.

Beam URB1 is an ordinary under-reinforced concrete beam with no external steel plate reinforcement and sufficient shear reinforcement to ensure a ductile flexural type failure. Beams URB2, URB3 and URB4 are similar to URB1 except that a steel plate of 1.5mm, 3mm and 5mm reinforced each beam, respectively. In all beams the epoxy glue thickness is fixed at 3mm. The material properties used in the model were identical to those reported in the experimental investigation. The finite element used parameter as shown in Table 1.

Table 1 Materials of concrete, plate, internal steel bar and epoxy

	Concrete			Internal steel bar			Plate				Epoxy
	f'_c (kg/cm ²)	ν	α	Yield stress (kg/cm ²)			Thickness (mm)	σ_y (kg/cm ²)	E (kg/cm ²)	ν	
URB1	549	0.2	0.189	D10	D08	D06	-				$E = 2842 \text{kg/cm}^2$ $\nu = 0.16$ $\phi = 28^\circ$ $C = 76 \text{kg/cm}^2$ $f_{i,s} = 120 \text{kg/cm}^2$ $f_{t,n} = \text{tensile strength of concrete}$
URB2	549		0.189	5400	5000	5000	1.5	2446	2040000	0.3	
URB3	843		0.045				3	2681			
URB4	549		0.189				5	2217			

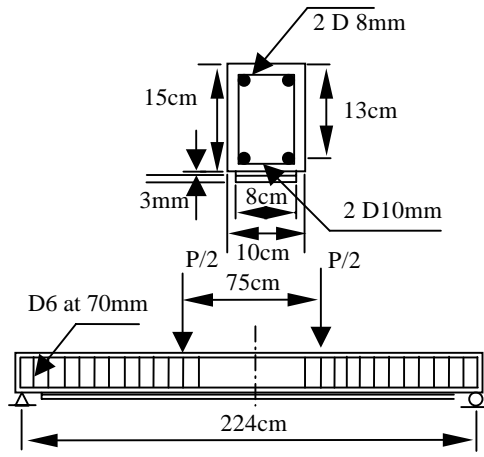


Fig. 11 Detail of RC strengthened beam

Result and Discussion

Ultimate load

Table 2 shows the comparison between numerical and reported experimental value of the ultimate loads for the various beams under study. Test results show close correlation between ultimate loads based on the finite element estimation and those obtained experimentally. The flexural capacity of beam URB1 is obtained from the strength theory based on the ACI code [27]. No code formulations exist presently for predicting ultimate capacities of RC beams strengthened with bonded steel plates. In this study, the RC beams strengthened with bonded steel plates will be predicted by strain compatibility. The ultimate flexural strength of the plated beams can be divided into the unplated RC beam and strengthened plate, respectively. For RC part, flexural ultimate strength was calculated by ACI code. For strengthened part, assuming the plate stress-strain is elastic-perfectly-plastic for tension and compression and the glue was neglected contribution. The predicted and experimental ultimate moments are shown and compared in Table 2. The results of Table 2 shows that the flexural ultimate strength of plated and unplated beams can be predicted satisfactorily by finite element and strain compatibility methods. Because the internal steel bar was modeled in elastic plastic with linear strain hardening after yielding, and the actual behavior of the internal steel bar may be strain hardening, but it is assumed in elastic-perfectly-plastic behavior in strain compatibility method. Hence, the ultimate load predicted by strain compatibility method is lower than the experimental results and the one predicted by finite element method.

Table 2 Ultimate loads of beam study

Beam	Plate thickness (mm)	Ultimate load (kg)		
		Finite element	Experiment	Strain compatibility
URB1	—	2886	2864	2763
URB2	1.5	3980	4077	3833
URB3	3	5459	5606	5245
URB4	5	5896	5861	5825

Load-deflection curve

Figure 12 shows comparison between the numerical and experimental load-deflection curve indicating reasonably close agreement.

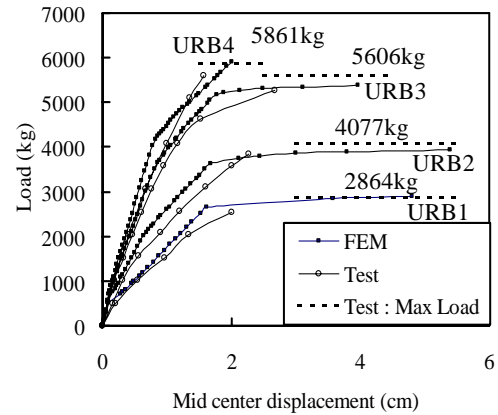


Fig. 12 Load deflection characteristics

Stress

Figures 13 and 14 show the tensile stress distribution in the internal steel bar and the external steel plates for beams URB2 and URB4 respectively, at ultimate load conditions as predicted by the finite element. Figure 13 exhibits that both the internal steel bar and the external steel plates for beams URB2 are yielded, indicating a flexure failure without separation. As shown in Fig. 14, the external steel plates of beam URB4 are yielded, but the internal steel bar remains elastic. Compare Fig. 13 with Fig. 14, the stress in the internal steel bar near the plate curtailment increased when the thickness of plates increased. The tensile force was transferred from the external plate to the internal steel bar near the plate curtailment when the plate was separated at the plate cut off.

Figure 15 shows the interface stress distribution predicted by finite element method and compare the analysis results by Roberts [6] in elastic range, and close agreement is indicated. It confirms that the program is correctness for interface element.

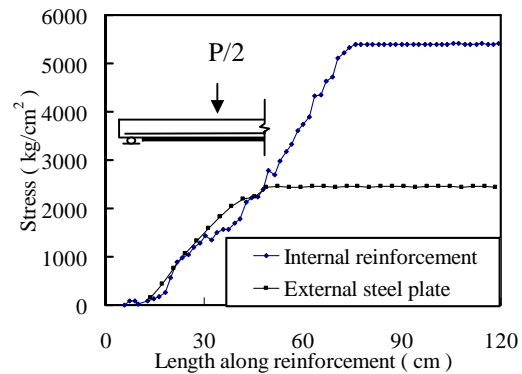


Fig. 13 Normal stresses distribution for URB2 at ultimate load

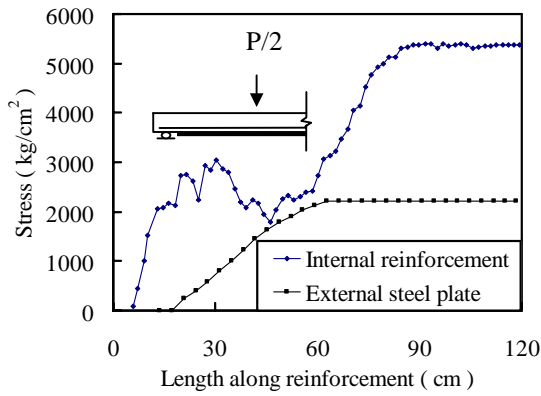


Fig. 14 Normal stresses distribution for URB4 at ultimate load

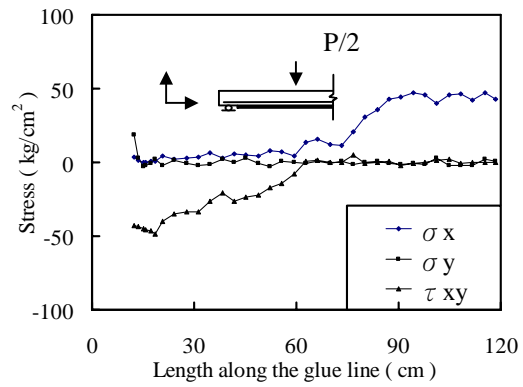


Fig. 17 Interface stress distribution for URB3 at ultimate load

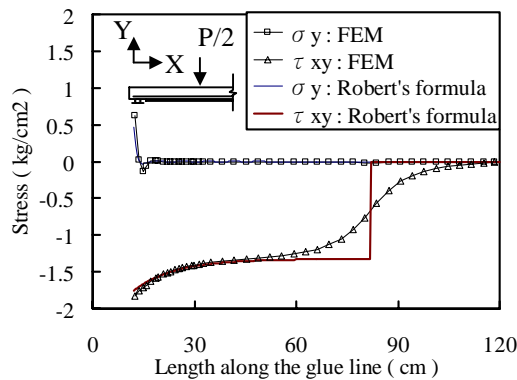


Fig. 15 Comparison interface stress distribution for URB3 at 896kg

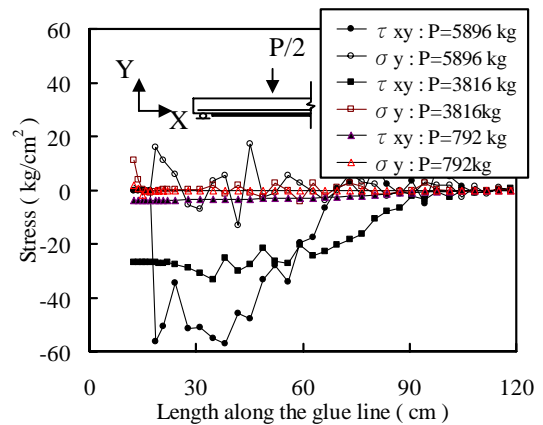


Fig. 18 Interface stress distribution for URB4 at various loads

Figures 16 to 18 show the interface normal and shear stresses for beams URB2, URB3, and URB4, respectively, as predicted by the finite element. As shown in Fig. 18, the value of interface stresses at various load for sampling Gauss points near the end of plate was higher than the value calculated by Mohr-Coulomb fracture criterion to indicate a plate separation in this region. The separation length of steel plate at various loading was shown in Fig. 19. On the contrary, the Beams URB2 and URB3 are not separation as shown in Figs. 16 and 17. Compare Fig. 16 with Fig. 17, the interface normal and shear stresses increased when the thickness of plates increased.

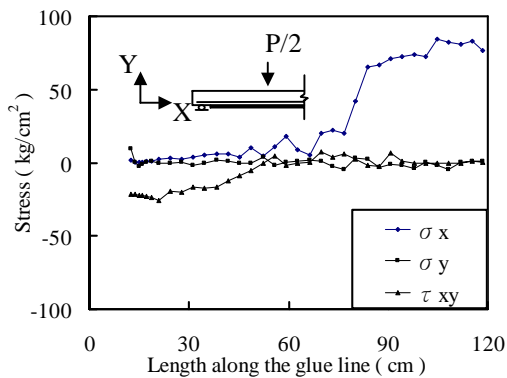


Fig. 16 Interface stress distribution for URB2 at ultimate load

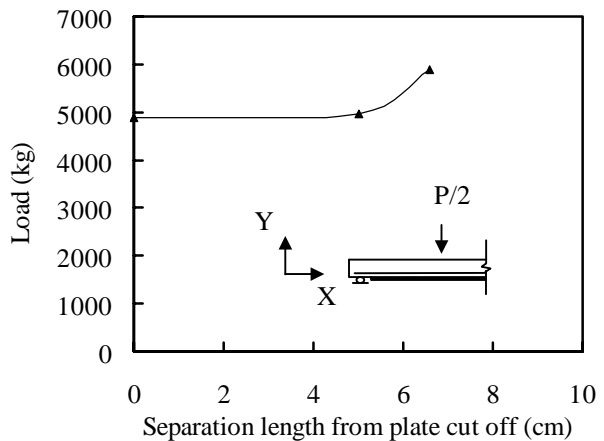


Fig. 19 Separation length for URB4 at various loads

Effect of interface cohesion c

In order to study the effect of the interface strength on the ultimate failure mechanism of beams bonded with thicker plates, the beam URB4 was analyzed by finite element method with different magnitudes of interface cohesion. Table 3 presents the ultimate load corresponding to different levels of cohesion. Beyond the 76kg/cm² value of cohesion, the interface is full

composite at ultimate load condition and the beam failed in flexure-shear mode, and both the internal steel bar and the external plates were yielding at ultimate load condition. For values of cohesion lower than 76kg/cm^2 , the beam fail in plate separation, and the internal steel bar was not yielding at plate separation. In order to confirm that the interface is full composite at ultimate load condition for certain interface cohesion, the beam URB4 was analyzed by finite element method without interface element. The value 5946kg of ultimate load was obtained for the model without interface element. This value is smaller 2.84% than the case for the model with interface element with $c = 120\text{kg/cm}^2$. It was affected by a reduced depth of the beam due to the absence of the 3mm interface layer.

Table 3 Effect of interface cohesion c on the ultimate load for URB4

Interface cohesion c (kg/cm^2)	Ultimate load P_u (kg)	Failure mode
40	4038	Plate separation
60	4880	Plate separation
76	5896	Plate separation
120	6120	Flexure
No interface element	5946	Flexure

Failure mode and cracking pattern

Figures 20 and 21 show the concrete cracking pattern at various loading for Beam URB2 and URB4, respectively. The cracking in constant moment region of Beam URB2 at ultimate loading display extensive vertical cracking and near the top of beam, but Beam URB4 is not. Beam URB4 display inclined cracking from the region of plate cut off. Table 4 presents the failure mode and states of internal steel bar, external steel plate, and interface at ultimate load condition. For beams bonded with thin plates, failure is full composite and yielding at both internal steel bar and external steel plate. For beam bonded thicker plates, failure occurs with plate separation and without the yielding of the external steel plate.

Table 4 Failure mode of beam study

Beam	Finite element			Experiment observation
	Internal steel	External plate	Interface	
URB1	Yielding IYZ = 41.5cm	-	-	Yielding of internal steel
URB2	Yielding IYZ = 45.0cm	Yielding EYZ = 76.5cm	No separation SZ = 0cm	Yielding of both internal steel and external plate
URB3	Yielding IYZ = 45.5cm	Yielding EYZ = 60.5cm	No separation SZ = 0cm	Yielding of both internal steel and external plate
URB4	No yielding IYZ = 0cm	yielding EYZ = 59.0cm	Separation SZ = 6.6cm	Yielding of external plate but not internal steel plate separation at curtailment

Note : IYZ = length of yielding of internal steel from center line.
EYZ = length of yielding of external plate from center line.
SZ = length of separation of epoxy from curtailment of plate.

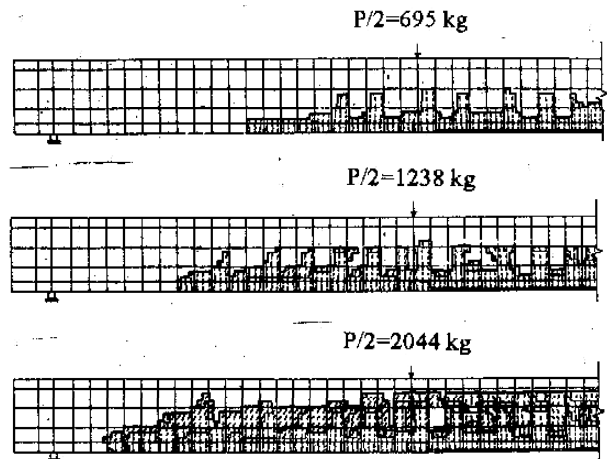


Fig. 20 Concrete cracking pattern for Beam URB2

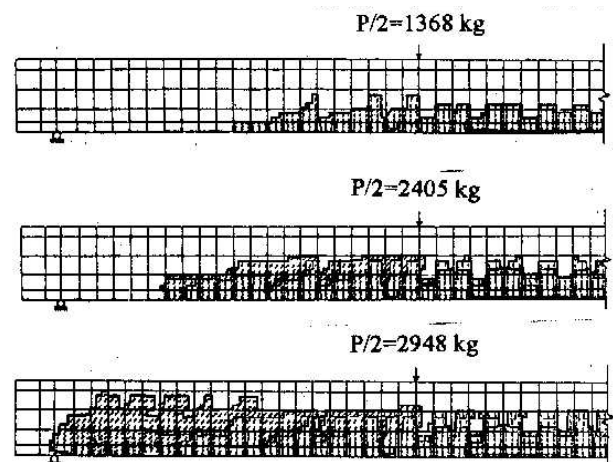


Fig. 21 Concrete cracking pattern for Beam URB4

5. CONCLUSIONS

Some important conclusions can be drawn based on the study results:

1. By comparing finite element solution with plastic theory, the internal steel bar using truss element and the external steel plates using deformation theory of plastic have been confirmed.
2. A nonlinear finite element method to predict response of RC beams strengthened by epoxy bonded steel plates can capture the essential characteristic of flexural behavior up to failure.
3. The interface element can pick up the shear and normal stress concentration at the plate curtailment, and also can judge separation if the peak shear and normal stress are exceeded.
4. An under-reinforced RC beam strengthened by external steel plate with thinner thickness is failed in a manner similar to a typical unplated under-reinforced RC beam. Both the internal steel bar and external steel plates are yielded at ultimate load condition. As

thickness of plate increasing, the peak normal and shear stress will be increased in the plate curtailment, and failure is plate separation if shear and normal stress as exceed Mohr-Coulomb type fracture criterion.

5. If the plate separation does not take place, the ultimate flexural strength of the plated beams can be predicted by strain compatibility, the strength of plated beam is the sum of the unplated RC beam and the strengthened plate. For RC part, flexural ultimate strength was calculated by ACI code. For strengthened part, the plate stress-strain is assumed as elastic-perfectly-plastic for tension and compression and the contribution of glue was neglected.
6. For insufficient interface strength between the concrete and external plate, the beam failed in separation of plate immediately. For sufficient interface strength, the beam is full composite at ultimate load with yielding at both internal and external reinforcing.
7. To avoid separation at the plate curtailment, the peak shear and normal stress concentration at the plate curtailment must be reduced. For this purpose, the plate must be anchored at the plate curtailment; the finite element analysis should extend to three-dimensional analysis.

REFERENCES

1. Swamy, R. N., Jones, R. and Charif, A., "The Effect of External Plate Reinforcement on the Strengthening of Structurally Damaged RC Beams," *Structural Engineer*, 67(3), pp. 45–56 (1989).
2. Swamy, R. N., Jones, R. and Bloxham, J. W., "Structural Behavior of Reinforced Concrete Beams Strengthened by Epoxy-Bonded Steel Plates," *Structural Engineer*, 65(2), pp. 59–68 (1987).
3. Ryback, M., "Reinforcement of Bridge by Gluing of Reinforcing Steel," *Materials and Structures*, 16(91), pp. 13–17 (1981).
4. Iino, T. and Otokawa, K., "Application of Epoxy Resins in Strengthening of Concrete Structures," *Proc. 3rd International Congress on Polymers in Concrete*, Koriyama, Japan, pp. 997–1011 (1981).
5. Jones, R., Swamy, R. N. and Charif, A., "Plate Separation and Anchorage of Reinforced Concrete Beams Strengthened by Epoxy-Bonded Steel Plates," *Structural Engineer*, 66(5), pp. 85–94 (1988).
6. Roberts, T. M., "Approximate Analysis of Shear and Normal Stress Concentrations in the Adhesive Layer of Plated RC Beams," *Structural Engineer*, 67(12), pp. 229–233 (1989).
7. Raphael, J. M., "Tensile Strength of Concrete," *ACI Journal*, 81(2), pp. 158–165 (1984).
8. Hillerborg, A., Modeer, M. and Petersson, P. E., "Analysis of Crack Formation and Crack Growth in Concrete by Means of Fracture Mechanics and Finite Elements," *Cement and Concrete Research*, 6(6), pp. 773–781 (1976).
9. Bergan, P. G. and Holand, I., "Nonlinear Finite Element Analysis of Concrete Structures," *Computer Methods Applied Mechanics Engineering*, 17(2), pp. 443–467 (1979).
10. Ziraba, Y. N. and Baluch, M. H., "Computational Model for Reinforced Concrete Beams Strengthened by Epoxy Bonded Steel Plates," *Finite Element in Analysis and Design*, 20(4), pp. 253–271 (1995).
11. Mphonde, A. G. and Frantz, G. G., "Shear Tests of High- and Low-Strength Concrete Beams without Stirrups," *ACI Journal*, 81(4), pp. 350–357 (1984).
12. Fenwick, R. C. and Paulay, T., "Mechanics of Shear Resistance of Concrete Beams," *Journal of the Structural Division*, 94(10), pp. 2325–2350 (1968).
13. Cedolin, L. and Poli, S. D., "Finite Element Studies of Shear-Critical R/C Beams," *Journal of Engineering Mechanical Division*, 103(3), pp. 395–410 (1977).
14. Kupfer, H. and Gerstle, K. H., "Behavior of Concrete under Biaxial Stresses," *Journal of Engineering Mechanical Division*, 99(4), pp. 853–866 (1973).
15. Guo, Z. H., Guo, Y. T., Yan, X., Ye, X. G. and Li, W. H., "Nonlinear Elastic Orthotropic Constitutive Model for Concrete," *Journal of Tsinghua University*, 37(6), pp. 78–81 (1997).
16. ACI Committee 363 "State-Of-The-Art Report on High Strength Concrete," *ACI Journal*, 84(4), pp. 361–411 (1984).
17. Massicottee, B., Elwi, A. E. and MacGregor, J. C., "Tension-Stiffening Model for Planar Reinforced Concrete Member," *Journal of Structural Engineering*, 116(11), pp. 3039–3058 (1990).
18. Vecchio, F. J. and Collins, M. P., "Modified Compression Field Theory for Reinforced Concrete Elements Subjected to Shear," *ACI Journal*, 83(2), pp. 219–231 (1986).
19. Vecchio, F. J. and Collins, M. P., "Compression Response of Cracked Reinforced Concrete," *Journal of Structural Engineering*, 119(12), pp. 3590–3610 (1993).
20. Belarbi, A. and Hsu, T. C., "Constitutive Laws of Softened Concrete in Biaxial Tension-Compression," *ACI Structural Journal*, 92(5), pp. 562–573 (1995).
21. Darwin, D. and Pecknold, D. A., "Nonlinear Biaxial Law for Concrete," *Journal of the Engineering Mechanics Division*, 103(2), pp. 229–241 (1979).
22. Lin, W. S., "Study on RC Structures Strengthened by

- External Steel Plates,” Ph.D. Dissertation, National Taiwan University, Taiwan (2002).
23. Ziraba, Y. N., Baluch, M. H., Basunbul, I. A., Azad, A. K., Al-Sulaimani, G. J. and Sharif, A. M., “Combined Experimental-Numerical Approach to Characterization of Steel-Glue-Concrete Interface,” *Materials and Structures*, 28, pp. 518–525 (1995).
 24. Jones, R., Swamy, R. N. and Ang, T. H., “Under- and Over-Reinforced Concrete Beams with Glued Steel Plates,” *International Journal of Cement Composites and Lightweight Concrete*, 4(1), pp. 19–32 (1982).
 25. Kupfer, H., Hilsdorf, H. K. and Rusch, H., “Behavior of Concrete under Biaxial Stresses,” *ACI Journal*, 66(9), pp. 656–666 (1969).
 26. Tasuji, M. E., Slate, F. O. and Nilson, A. H., “Stress-Strain Response and Fracture of Concrete in Biaxial Loading,” *ACI Journal*, 75(7), pp. 306–312 (1978).
 27. ACI Committee 318, “Building Code Requirements for Structural Concrete (ACI 318 M-99) and Commentary (ACI 318 RM-99),” *American Concrete Institute*, Farmington Hills, p. 353 (1999).

(Manuscript received Mar. 22, 2001,
Accepted for publication June 20, 2003.)